Geoscientific
Model Development
Discussions

1 **A new temperature-photoperiod coupled phenology module in LPJ-**

2 **GUESS model v4.1: optimizing estimation of terrestrial carbon and**

3 **water processes**

4 Shouzhi Chen[1], Yongshuo H. Fu[1,2*], Mingwei Li[1], Zitong Jia[1], Yishuo Cui[1], Jing

5 Tang[3*]

6 [1]College of Water Sciences, Beijing Normal University, Beijing 100875, China.

7 [2]Plants and Ecosystems, Department of Biology, University of Antwerp, Antwerp,

8 Belgium.

9 [3] Department of Biology, University of Copenhagen, Denmark.

10

11 *Corresponding author*:

12 Yongshuo Fu (yfu@bnu.edu.cn); Jing Tang (jing.tang@bio.ku.dk).

13 **Abstract**

14 Vegetation phenological shifts impact the terrestrial carbon and water cycle, and affects

15 local climate system through biophysical and biochemical processes between biosphere

16 and atmosphere. Dynamic Global Vegetation Models (DGVMs), serving as pivotal

17 simulation tools for investigating terrestrial ecosystem carbon and water cycles,

18 typically incorporate representations of vegetation phenological processes.

19 Nevertheless, it is still a challenge to achieve accurate simulation of vegetation

20 phenology in the DGVMs. Here, we developed and coupled the spring and autumn

21 phenology models into one of the DGVMs, LPJ-GUESS. These process-based

22 phenology models driven by temperature and photoperiod, and are parameterized for

23 deciduous trees and shrubs using remote sensing-based phenological observations and

24 reanalysis dataset ERA5 land. The results show that the developed LPJ-GUESS with

Geoscientific
Model Development
Discussions
Open Access
EGU

25   new phenology modules substantially improved the accuracy in capturing start and end

26   dates of growing seasons. For the start of growing season, the simulated RMSE for

27   deciduous tree and shrubs decreased by 8.04 and 17.34, respectively. For the autumn

28   phenology, the simulated RMSE for deciduous tree and shrubs decreased by 22.61 and

29   17.60, respectively. Interestingly, we have also found that differences in simulated start

30   and end of growing season can largely alter the ecological niches and competitive

31   relationships among different plant functional types (PFTs), and subsequentially impact

32   the community structure and in turn influence the terrestrial carbon and water cycles.

33   Hence, our study highlights the importance getting accurate of phenology estimation to

34   reduce the uncertainties in plant distribution and terrestrial carbon and water cycling.

35   **Keywords:** LPJ-GUESS, phenology model, model modification, ecological processes

1. Introduction

36

37   Vegetation plays a pivotal role within the terrestrial ecosystem, as the interplay

38   between vegetation and climate exerts significant influence on the mass and energy

39   cycles across a broad range of temporal and spatial scales (Zhu et al., 2016; Piao et al.,

40   2019; Chen et al., 2022a). In recent years, with the increase of carbon dioxide

41   concentration and land surface temperature, significant vegetation greening has been

42   reported world widely, and the annual growth dynamics of vegetation have undergone

43   significant changes, especially the spring and autumn phenological changes (Zhu et al.,

44   2016). A large amount of research evidences have indicated that climate change results

45   in the advancement of spring phenology and the postponement of autumn phenology,

46   exerting a profound influence on the carbon and water cycles within terrestrial

47   ecosystems (Piao et al., 2019; Badeck et al., 2004; Zhou et al., 2020), and the

48   geographic distribution of species (Chuine, 2010; Fang and Lechowicz, 2006; Huang

49   et al., 2017). Under conditions of sufficient water supply and no radiation constraints,

50   the extension of the growing season resulting from vegetation phenological shifts will

51   contribute additional carbon sinks to terrestrial ecosystems (Zhang et al., 2020; Keenan

52   et al., 2014). Longer growing seasons also lead to greater evapotranspiration, mainly in

53   early spring and autumn, which in turn reduces watershed runoff (Huang et al., 2017;

54   Kim et al., 2018; Chen et al., 2022b; Geng et al., 2020). Nevertheless, it is still a

55   challenge to achieve accurate simulation of vegetation phenology in dynamic global

56   vegetation models (DGVMs), especially in the context of climate change (Richardson

57   et al., 2012). We urgingly caution that improving the vegetation phenology module of

58   DGVMs, and taking the response of vegetation phenology to climate change into

59   consider comprehensively, which is a necessary development to improve model

60   simulation accuracy and reduce model uncertainty.

61   The State-of-the-art DGVMs generally include phenology modules in vegetation

62   submodels, but the implementations vary widely, which include: 1) using fixed and

63   prescribed seasonal dynamics to characterize phenology, and the models using this

64   method include SiB model, SiBCASA model, ISAM model, etc. (Sellers et al., 1986;

65   Schaefer et al., 2008; Jain and Yang, 2005); 2) using remote sensing data or in-situ

66   observations directly describing the vegetation growth dynamics instead of process-

67   based simulation, SiB2, BEPS and ED2 are all based on this method to describe the

68   vegetation growth dynamics (Sellers et al., 1996; Deng et al., 2006; Medvigy et al.,

69   2009); 3) using vegetation phenology model which take the response of vegetation

70   biophysiology to environment factors into account to simulate vegetation growth

71   dynamics. In comparison to the first two methods, the third approach offers the

72   advantage of depicting the responses of vegetation to the external environment

73   grounded in plant physiological processes , and can trace the dynamics of vegetation

74   growth amidst changing environment conditions, so it is adopted by several DGVMs,

75   e.g. Biome-BGC, ORCHIDEE and LPJ-GUESS (Thornton et al., 2002; Krinner et al.,

76   2005; Sitch et al., 2003). With the evolving comprehension of the intricate response

77   mechanisms of vegetation to external environment, vegetation phenological models

78   have experienced substantial advancements in recent decades, which encompass shifts

79   from single-process to multi-process mechanisms and from single-variable to multi-

80   factor model constraints. (Liu et al., 2018; Fu et al., 2020; Piao et al., 2019). For spring

81   phenological models, in the early stage, temperature was the only factor considered,

82   resulting in relatively simplistic model processes, which was also commonly adopted

83   by DGVMs (GDD and Unified etc.) (Sarvas, 1972; Chuine, 2000). With the deepening

84   of the understanding of spring phenological mechanism, factors such as radiation and

85   photoperiod have been introduced into the phenological model, and the corresponding

86   complex regulatory mechanisms have also been perfected, e.g. Sequential model,

87   Parallel model and DROMPHOT model etc. (Hänninen, 1990; Kramer, 1994; Caffarra

88   et al., 2011). As for the autumn phenological model, the early model form was also

89   relatively simple (cold temperature-driven CDD model) but widely used in DGVMs,

90   and some DGVMs used fixed leaf longevity for determination of autumn phenological

91   dates. The development of relatively complex autumn phenological mechanism models

92   is relatively late, and these advanced autumn phenological models take photoperiod and

93   carbon accumulation into account in the model process, such as DM model,

94   photosynthesis-influenced autumn phenology (PIA) model (Zani et al., 2020; Delpierre

95   et al., 2009). Many researches have pointed out that early phenological models tend to

96   be overly simplistic and result in biased predictions, which indicates that the vegetation

97   phenological models of DGVMs need to be updated urgently (Kucharik et al., 2006;

98   Ryu et al., 2008). The use of more accurate phenological models covering more

99   complex mechanisms is of great significance to reduce the simulation errors of DGVMs

100   and improve the simulation reliability under future climate warming.

101   In this study, we used the remote sensing-based phenology data together with

102   threshold and maximum rate of change method to parameterize the spring

103   DROMPHOT model and autumn DM model for boreal needle leaved summergreen tree

104   (BNS), Shade-intolerant broadleaved summergreen tree (IBS), shade-tolerant

105   temperate broadleaved summergreen tree (TeBS) and summergreen shrubs plant

106   function types (PFTs). The new phenology module with these parameters were coupled

107   into the LPJ-GUESS model. The objectives of this study are as follows:1) to couple

108   more mechanistic phenology modules into LPJ-GUESS to improve the accuracy of

109   spring and autumn phenology simulations; (2) to assess the impacts of different

110   vegetation phenological algorithms on the carbon and water process simulations.

111   **2. Materials and methods**

112   **2.1 Datasets**

113   **2.1.1 GIMMS NDVI$_{4g}$**

114   Normalized differential vegetation index (NDVI) is commonly used as a proxy for

115   vegetation canopy greenness and growth condition. In the study, we used the forth-

116   generation NDVI dataset of GIMMS, which provides biweekly NDVI records with a

117   spatial resolution of 1/12° (~8 km), during 1982-2017 to extract the start and end of

118   growing season (Pinzon and Tucker, 2014; Tucker et al., 2005; Cao et al., 2023). This

119   NDVI dataset has been refined and corrected for orbital drift, calibration, viewing

120   geometry, and volcanic aerosols, which can accurately reflect the accurate growth

121   dynamics of surface vegetation (Kaufmann et al., 2000).

122   **2.1.2 ERA5-land daily air temperature**

123   The ERA5-Land daily air temperature dataset has been used to parameterize spring

124   and autumn phenological algorithms and force LPJ-GUESS model. The dataset is a

125   global reanalysis dataset developed by the European Centre for Medium-Range

126   Weather Forecasts (ECMWF), which utilises advanced data assimilation techniques

127   combining observations from various sources, such as satellites, weather stations, and

128   weather balloons, with numerical weather prediction models. We downloaded the

129   ERA5 land daily air temperature at 0.5° spatial resolution (consistent with CRU NCDP

130   data,   from   1982-2015)   from   their   official   website

131   (https://cds.climate.copernicus.eu/cdsapp#!/dataset/reanalysis-era5-land?tab=form).

132   Due to possible bias between different data sets, we calculated the monthly average of

133   ERA5 land daily air temperature and calculated its climatology, as well as climatology

134   of CRU NCEP monthly air temperature data, and corrected the bias of ERA5 land data

135   according to the deviation.

136   **2.1.3 GLC 2000 land cover data**

137   Satellite remote sensing can capture the collective information from mixed pixels

138   comprised of various plants and also information from dominant vegetation. The data

139   acquired through satellite remote sensing can be regarded as representative of a

140   particular vegetation type only when the plant functional types within a gridcell exhibit

141   a relatively homogeneous composition. Based on GLC2000 land cover types data,

142   which are designated according to PFTs ascribed to satellite images and ground-truth

143   by regional analysts with 1 km spatial resolution (Bartholome and Belward, 2005), we

144   calculated the proportion of different PFTs in the 0.5°×0.5° gridcell to identify pixels

Geoscientific
Model Development
Discussions

145   dominated by a specific plant functional type (the proportion of a specific plant function

146   type is greater than 50%, Fig. 1 and Fig. S1).
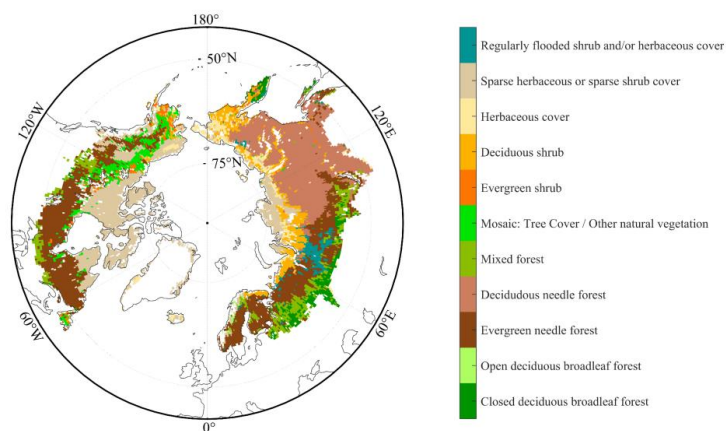
147   **Figure 1**. **The spatial distributions of 11 detailed regional land-cover types in the**
148   **GLC2000 products.** BNS: Deciduous needle forest, IBS&TeBS: Open deciduous
149   broadleaf forest and closed deciduous broadleaf forest, Shrubs: Sparse herbaceous or
150   sparse shrub cover and Deciduous shrub.

151   **2.2 Phenology dates extraction**

152   We used five phenological extraction methods, which includes three threshold-

153   based methods (i.e. Gaussian-Midpoint, Spline-Midpoint and Timesat-SG Methods)

154   and two change rate-based methods (i.e. the HANTS-Maximum and Polyfit-Maximum

155   methods) following previous studies (Cong et al., 2012; Savitzky and Golay, 1964;

156   Chen et al., 2023), to retrieval spring (start of growing season, SOS) and autumn (end

157   of growing season, EOS) phenological events (Fig.S2). Phenological extraction based

158   on multiple methods consists of three steps: 1) smoothing and interpolating the NDVI

159   date to obtain the smooth and continuous NDVI daily time series; 2) using the threshold

160   value (0.5 for SOS and 0.2 for EOS) or the maximum rate of change to extract the

8

161 vegetation phenology from each single method (Reed et al., 1994; White et al., 1997;

162 White et al., 2009; Piao et al., 2006); 3) averaging the phenological results obtained by

163 different extraction methods to reduce uncertainties associated with a single method

164 (Due to the different fitting methods, interpolation methods and threshold settings of

165 different extraction methods) (Fu et al., 2021; Fu et al., 2023).

166 **2.3 Model description**

167 LPJ-GUESS is a process-based dynamic global vegetation model that can

168 simulate vegetation dynamics and soil biogeochemical processes across different

169 terrestrial ecosystems. At gridcell level, the model simulates vegetation growth,

170 allometry competition, mortality and disturbances (Sitch et al., 2003; Morales et al.,

171 2005; Hickler et al., 2004). The PFTs within the framework of the LPJ-GUESS model

172 encapsulate the extensive spectrum of structural and functional attributes

173 characteristic of potential plant species. Within a given area (patch, corresponding in

174 size approximately to the maximum area of influence of one large adult individual on

175 its neighbors), plant growth is governed by the synergistic interplay of bioclimatic

176 constraints and interspecific competition for spatial dominance, access to light, and

177 vital resources. In a gridcell (stand), it's typically simulating multiple such patches

178 to represent different disturbance histories within a landscape, and across these

179 patches, the modeled properties tend to coalesce towards a singular, overarching

180 average value.

181 In LPJ-GUESS model, spring phenology is calculated based on spring heat and

182 winter cold requirements (Sykes et al., 1996). Plants have certain energy

183 requirements for budburst, which are expressed by using growing degree days above

184 5 degrees (GDD5), while growing degree days to budburst is also related to the length

185 of the chilling period. An increase in chilling periods can reduce the requirement for

186 growing degree days to budburst, in other words, budburst can be delayed long

187 enough to minimize the risk that the emerging buds will be damaged by frost

188 (Equation 1):

$$GDD = a + b \times e^{-k \times C} \tag{1}$$

189 Where a, b and k are PFT-specific constants, and C is the length of chilling

190 period. GDD represents the growing degree days requirement of a specific PFT at a

191 chilling period length of C. Growing degree days are defined as the accumulation of

192 temperatures above the base temperature (generally 5 ℃), and the length of chilling

193 period is defined as the days that daily mean temperature below 5 ℃.

194 For autumn phenology, leaf longevity was used as a threshold in the LPJ-

195 GUESS model for the simple prediction of senescence. It is assumed in the model

196 that autumn phenology occurs when the cumulative complete leaf longevity is greater

197 than 210 days or the daily average temperature below 5℃ in autumn.

198 Within each stand, 50 different patches (in this study) were applied to represent

199 different disturbance histories within a landscape. The simulations over the study

200 areas included 23 PFTs, which consist of five grass, three bryophytes, eight shrubs

201 and seven tree PFTs, and the summergreen PFTs involved in the improvement of

202 vegetation phenological simulation contain BNS, IBS, TeBS and deciduous shrubs

203 (hereafter called Shrubs), see detailed description in Tang et al. (2023) and Rinnan et

204   al. (2020).

2.4 LPJ-GUESS phenology module modification

206   We improved the spring and autumn phenological modules of the LPJ-GUESS

207   model by coupling DROMPHOT model and DM model into LPJ-GUESS according to

208   the phenological module improvement flow chart (Fig.2).
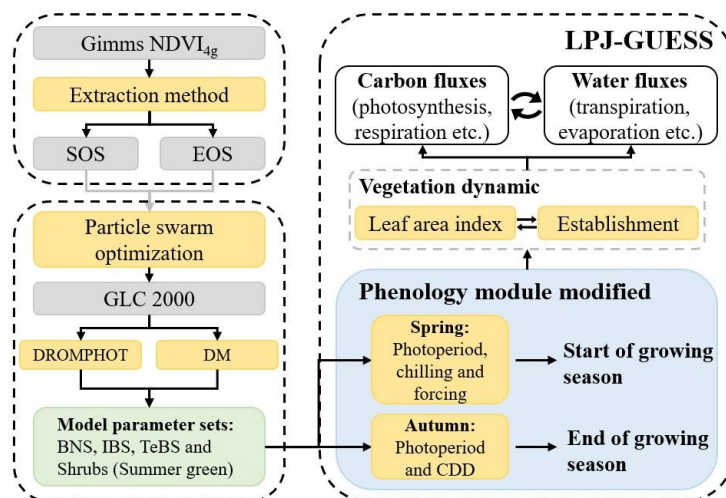
**Figure 2 Flowchart of spring and autumn phenological module modification in
LPJ-GUESS.** Dotted boxes represent independent work, gray boxes represent different
data sets or intermediate process results, and yellow boxes represent different
calculation methods or model modules. CDD, cold degree days.

213   The spring phenological model in LPJ-GUESS was replaced by DROMPHOT

214   model, which introduces the effect of photoperiod on dormancy, and further refined the

215   spring phenological model into three stages: dormancy induction, dormancy release and

216   growth resumption (Caffarra et al., 2011). The dormancy induction process is triggered

217   by a short photoperiod (DR_P) and a low temperature (DR_T), and finishes when the

218   cumulant of the product of DR_P and DR_T reaches a specific threshold ($DS > D_{crit}$,

219   Equation 2, 3 and 4):

$$DS = \sum_{t_0}^{t} DR_T \times DR_P \qquad (2)$$

$$DR_T = \frac{1}{1 + e^{aD \times (T - bD)}} \qquad (3)$$

$$DR_P = \frac{1}{1 + e^{10 \times (DL - DL_{crit})}} \qquad (4)$$

220   Where t_0 is the start date of dormancy induction, which defined at September 1st

221   of the year preceding budburst, DS represents the state of dormancy induction (the

222   cumulant of daily photoperiod, i.e. DR_P, and temperature, i.e. DR_T, effect), T is the

223   daily mean temperature, and DL is day length on day t. aD, bD and DL_{crit} are model

224   parameters that regulate the effect of photoperiod and temperature.

225   Dormancy release and growth resumption start after dormancy induction is

226   complete (t_d), which represent a parallel chilling and forcing process, respectively. The

227   total daily rate of chilling (S_C) is defined as the accumulation of daily chilling (R_C) as

228   Equation 5, and the daily forcing (R_f) is determined by both photoperiod and S_C

229   (Equation 6, 7 and 8), that the effect of photoperiod and chilling on R_f counteracts each

230   other. The increase of photoperiod will decrease R_f while the increase of chilling will

231   reverse the effect:

$$S_C = \sum_{t_d}^{t} R_C = \sum_{t_d}^{t} \frac{1}{1 + e^{aC \times (T - cC)^2 + (T - cC)}} \qquad (5)$$

12

Geoscientific
Model Development
Discussions

EGU

$$DL_{50} = \frac{24}{1 + e^{hDL \times (S_C - C_{crit})}} \qquad (6)$$

$$T_{50} = \frac{60}{1 + e^{gT \times (DL - DL_{50})}} \qquad (7)$$

$$S_f = \sum_{t_d}^{t} R_f = \sum_{t_d}^{t} \frac{1}{1 + e^{dF \times (T - T_{50})}} \qquad (8)$$

232   Where aC, cC and C_{crit} are the model parameters of chilling process, and hDL, gT

233   and dF are the model parameters of forcing process. When the total daily rate of forcing

234   (S_f) reaches a critical value F_{crit}, vegetation completely resumes growth and spring

235   phenological events occurred. Note that gT and hDL must be greater than zero to limit

236   the monotonicity of Equation 6 and 7.

237   Since the lack of process based submodule to simulate autumn phenology in LPJ-

238   GUESS model, and only a fixed leaf longevity is used to define occurrence date of

239   autumn phenology, we introduced autumn phenology process that considers

240   photoperiod and cold temperature effects by coupling the DM model into the LPJ-

241   GUESS model (Delpierre et al., 2009). The DM model assumes that plants will respond

242   to low temperature (below base temperature, T_b) only when the photoperiod is below a

243   critical value (DL_{crit}), and the daily rate of senescence (R_{sen}) on that day is determined

244   by cold temperature and photoperiod (Equation 9,10 and 11):

$$f(DL) = \alpha_{pn} \times \frac{DL}{DL_{crit}} + (1 - \alpha_{pn}) \times \left(1 - \frac{DL}{DL_{crit}}\right), \ \alpha_{pn} \in \{0,1\} \qquad (9)$$

$$R_{sen} = \begin{cases} 0, & DL \geq DL_{crit} \\ 0, & DL < DL_{crit} \ \& \ T \geq T_b \\ (T_b - T)^x \times f(DL)^y, & DL < DL_{crit} \ \& \ T < T_b \end{cases} \quad (10)$$

$$S_{sen} = \sum_{t_0}^{t} R_{sen} \quad (11)$$

245   Where α_{pn} is a parameter determines that photoperiod shorter than the DL_{crit}

246   threshold weaken (α_{pn} equal to 1) or strength (α_{pn} equal to 0) the cold-degree sum effect.

247   x and y are the indices of the temperature and photoperiod terms in the formula, which

248   are used to adjust the degree of influence of temperature and photoperiod on Rsen,

249   respectively.

2.5 Phenological model parameterization

251   Utilizing the spatial distribution of predominantly homogeneous pixels

252   corresponding to distinct vegetation types, we partitioned the remote sensing

253   phenological dataset, and finally obtained the phenological dataset of BNS, IBS, TeBS

254   and Shrubs for the parameterization of DORMPHOT and DM models. We divided the

255   phenology dataset into two parts according to the odd or even number of years, the odd-

256   numbered years for model parameter calibration and the even-numbered years for

257   model validation. Particle swarm optimization (PSO) algorithm was applied to

258   parameterize the DROMPHOT and DM model for different PFTs, which used the

259   mixed function that comprehensively considers multiple evaluation indicators as the

260   objective function ($f(mixed)$, Equation 12), and sets the upper limit of iteration to

261   5000 times to find the global optimal parameter (Marini and Walczak, 2015; Poli et al.,

262 2007). The parameters of DROMPHOT model and DM model applicable to BNS,

263 IBS&TeBS and Shrubs PFTs were found by PSO algorithm (Table S1 and S2).

$$f(mixed) \ = \ 100*(1-R^2)+100*(1-NSE)+10*RMSE \tag{12}$$

264 Where R^2 is coefficient of determination, NSE is Nash–Sutcliffe Efficiency, and

265 RMSE is Root mean square error. The coefficients in front of each term of the formula

266 are used to adjust the weights of different evaluation indicators. The smaller the

267 objective function, the closer the simulated value of the model is to the observed value.

268 **2.6 Simulation set-up**

269 To compare the simulation performance of LPJ-GUESS which employing original

270 phenological module and modified phenological module (the extended LPJ-GUESS).

271 We first ran the model using CRU NCEP v7 gridded climate data

272 (https://rda.ucar.edu/datasets/ds314.3/) which includes monthly air temperature,

273 precipitation, wind speed, wet days, incoming shortwave radiation and relative

274 humidity over the period 1901-1978 with a 500 year spin up and saved all model state

275 variables at the end of 1978 (used the original phenological module, and the status

276 variables associated with the modified phenological module were also updated and

277 saved concurrently) to avoid the differences in the simulated vegetation and soil state

278 variables outside the study period, i.e. 1979-2015 (Viovy, 2018). Then we restarted the

279 model simulations (applying the original phenological module and modified

280 phenological module, respectively) with the saved model state variables at the last day

281 of 1978 and ERA5 land daily air temperature, note that other forcing data were still

282   from CRU NCEP v7 data set, and printed start (end) of growing season of summer

283   green PFTs, monthly grid level gross primary productivity (GPP) and actual

284   evapotranspiration (AET) of each PFT and foliar projection cover (FPC), for

285   investigating the simulation difference which induced by phenological simulation

286   differences.

287   **3. Results**

288   **3.1 Phenology simulation performance**

289   For spring phenology, DROMPHOT model has the best simulation performance

290   in the IBS&TeBS region (R^2 = 0.62 & NSE = 0.62), followed by in the regions

291   dominated by BNS (R^2 = 0.52 & NSE = 0.52) and Shrubs (R^2 = 0.47 & NSE = 0.47)

292   (Table 1). For autumn phenology the simulation performance was generally worse than

293   that of spring phenology. The DM model has the best simulation performance in the

294   Shrubs region, (R^2 = 0.39 & NSE = 0.39), followed by in the regions dominated by

295   BNS (R^2 = 0.33 & NSE = 0.32) and IBS&TeBS (R^2 = 0.47 & NSE = 0.47) (Table 1).

296   **Table 1 Model performances of DROMPHOT and DM models.**

Model	Plant function type	Calibration			Validation		
		R^2	NSE	RMSE	R^2	NSE	RMSE
DROMPHOT	BNS	0.54	0.53	7.71	0.52	0.52	7.96
	IBS&TeBS	0.61	0.61	7.92	0.62	0.62	7.91
	Shrub	0.45	0.44	11.3	0.47	0.47	11.1
DM	BNS	0.28	0.28	10.7	0.33	0.32	10.7
	IBS&TeBS	0.29	0.28	14.9	0.32	0.31	14.4
	Shrub	0.42	0.42	10.4	0.39	0.39	10.5

297   R^2, coefficient of determination, NSE, Nash–Sutcliffe Efficiency, RMSE, Root mean

298   square error. BNS, boreal needle leaved summergreen tree, IBS, Shade-intolerant

299   broadleaved summergreen tree, TeBS, shade-tolerant temperate broadleaved

300   summergreen tree and Shrubs, summergreen shrubs plant function types).

301

302   Compared with remote sensing-based vegetation phenological indices, LPJ-

303   GUESS with the original phenological module estimated earlier spring onset and

304   autumn leaf senescence. The simulated spring phenology matches better than that of

305   autumn phenology. The extended LPJ-GUESS model has greatly improved the

306   estimation accuracy in regions dominated by BNS, IBS&TeBS and Shrubs PFTs (Fig.

307   3 and Fig. S3). For spring phenology, the simulated R^2 (RMSE) of the extended LPJ-

308   GUESS model for regions dominated by BNS, IBS&TeBS and Shrubs PFTs were 0.53

309   (7.84), 0.46 (11.21) and 0.61 (7.92), respectively, which increased (decreased) by 0.26

310   (5.55), 0.25 (10.53) and 0.12 (17.34) compared with the original phenological module.

311   We found that PFTs with larger R^2 increase in spring phenological simulation also

312   had smaller RMSE reductions for the extended model, indicating the improvements in

313   capturing interannual change and the multi-year mean value. The autumn phenology

314   simulation performance with was greatly improved by integrating DM model for

315   regions dominated by BNS, IBS&TeBS and Shrubs PFTs, the simulated R^2 (RMSE) of

316   the extended LPJ-GUESS model were 0.31 (10.70), 0.41 (10.42) and 0.31 (14.69),

317   respectively, which increased (decreased) by 0.11 (15.66), 0.30 (29.56) and 0.29 (17.60).

318   By comparing the LPJ-GUESS simulated daily LAI before and after coupling the DM

319   model, we also found that the autumn LAI values simulated by the extended LPJ-

320   GUESS no longer suddenly decrease to 0 over a day, but rather smoothly decrease with

321   the sigmoid function according to the control of cold temperature and photoperiod (Fig.

322   S4).

Geoscientific
Model Development
Discussions
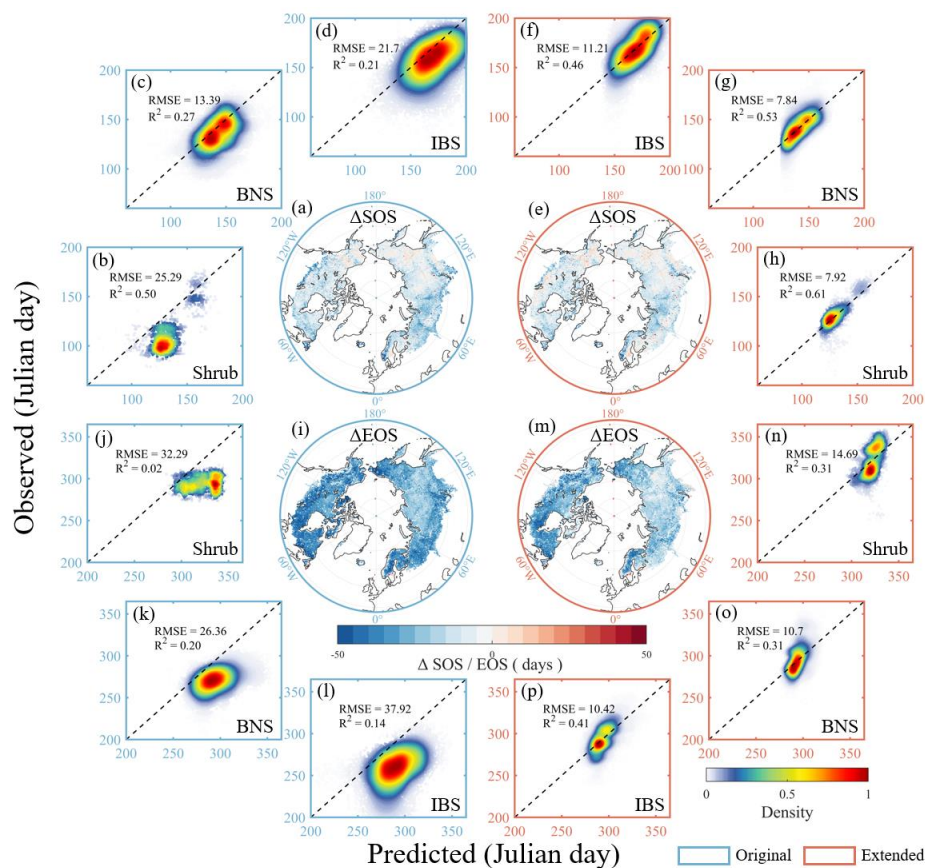
Figure 3 Comparison of the simulated performance of spring (SOS) and autumn (EOS) phenology between the original (left blue panels) and the extended (right red panels) LPJ-GUESS. (a-d) Simulation performance of SOS using the original LPJ-GUESS, (e-h) Simulation performance of SOS using the extended LPJ-GUESS, (i-l) Simulation performance of EOS using the original LPJ-GUESS, (m-p) Simulation performance of EOS using the extended LPJ-GUESS. Blue and red boxes represent spring and autumn phenological simulations. The spatial geographic map showed the difference between the simulation results of LPJ-GUESS model and the remote sensing phenology, with blue representing the model underestimation and red representing the model overestimation. The dotted lines in the subgraph are 1:1 line.

3.2 Gross primary productivity simulation

Since the PFTs simulated in LPJ-GUESS model include not only BNS, IBS&TeBS and Shrubs, but also evergreen plants and grass (no development was made to its phenological simulation in the present study), we found that clear differences between

337 two versions of the model mainly appeared in the regions dominated by these deciduous

338 PFTs with improved phenological modules. We only found small differences in the

339 regions dominated by evergreen or grassland (Fig. 4c). It is also clear that the original

340 LPJ-GUESS generally simulated higher GPP than the extended one over the study

341 period, except for the IBS&TeBS dominated regions, where higher GPP from the

342 original model can be only found from 1979 to 2000 (Fig. 4d-f). By comparing multiple

343 years' monthly mean GPP values, it becomes evident that the modified phenology also

344 influences the seasonal dynamics of GPP. In regions dominated by BNS, the differences

345 in monthly GPP are primarily noticeable during spring (using modified phenological

346 module resulted in a -34.9% lower GPP in May compared to original phenological

347 module, when not specifically stated, the value is that the extended model differs from

348 the original model, Fig. 4g). In regions dominated by IBS&TeBS, GPP differs in both

349 spring (-2.8%) and autumn (-6.3%) and the difference is larger in autumn, which mainly

350 contribute to annually GPP difference (Fig. 4h). In Shrubs dominate regions, we found

351 differences in GPP in all months (-43.9%), especially in the non-growing season,

352 indicating that some evergreen plants still exist in the region when the original

353 phenological module is used, and that changes in vegetation phenology seems

354 substantially affect vegetation composition in this region (Fig. 4i). Compared with

355 VPM GPP products, we also found that extended LPJ-GUESS model could simulate

356 GPP more accurately during transition periods (Fig. S5).

357

19

Geoscientific
Model Development
Discussions
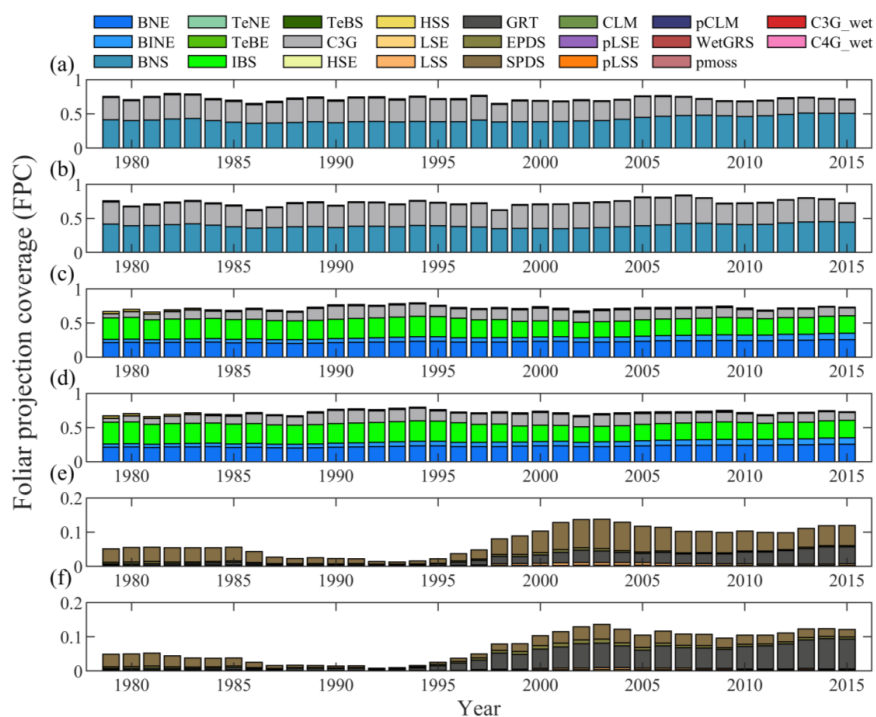
Figure 4 Comparison of gross primary productivity simulations between scenarios which used original phenological module and modified (DROMPHOT and DM) phenological module. (a) Scenario used original phenological module, (b) scenario used modified phenological module, and (c) the difference between the two scenario mentioned above, blue represents a larger simulation value for the LPJ-GUESS model using the original phenological module, and red is smaller. (d-f) Annual average GPP for BNS, IBS&TeBS and Shrubs PFTs from 1979 to 2015. (g-i) Multi-year mean monthly GPP for BNS, IBS&TeBS and Shrubs PFTs from 1979 to 2015.

The potential natural plant distribution also confirmed that the gridcells with large

differences in phenological simulations between original and extended LPJ-GUESS has

also large differences in dominant vegetation types (Fig. S3). We selected typical

gridcells in BNS, IBS&TeBS and Shrubs region, and compared their multi-year

variation pattern of FPC, it was found that phenological changes had a significant

20

Geoscientific
Model Development
Discussions

373 influence on FPC changes in BNS and Shrubs region (Fig. 5). However, in the

374 IBS&TeBS region (the gridcell dominated by IBS was selected here), although we

375 found that the difference in phenological simulation effects little on FPC components,

376 due to the close proportion of IBS and BNE (fierce competition), small changes in FPC

377 components could also lead to changes in dominant vegetation types (Fig. 5c, d).
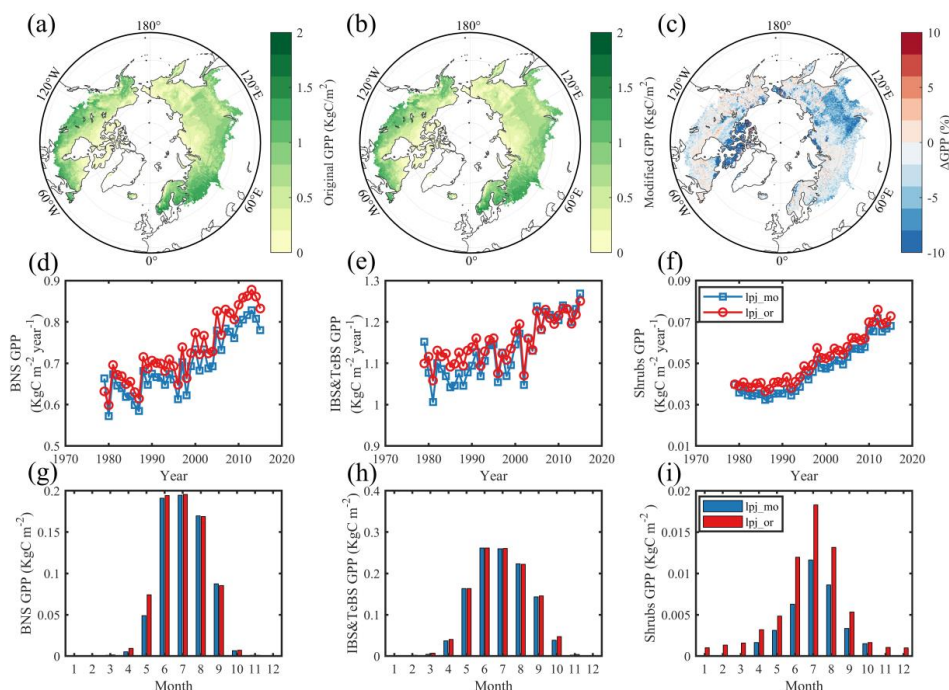
378 **Figure 5. Shifts of foliage projection coverage (FPC) of typical gridcell in the**
379 **regions dominated by BNS, IBS & TeBS and Shrubs PFTs over the period 1979 -**
380 **2015.** (a) BNS, (c) IBS&TeBS and (e) Shrubs typical gridcells used original LPJ-
381 GUESS model, (b) BNS, (d) IBS&TeBS and (f) Shrubs typical gridcells used extended
382 LPJ-GUESS model.

383 **3.3 Evapotranspiration simulation**

384   By comparing the spatial pattern, we found that BNS dominated the regions with

385 large differences in the modelled AET under the two runs, and the simulation result

386   using the original phenological module were significantly larger (3.9%) compared with

387   that using the modified module (Fig.6c). In the IBS&TeBS dominated region, like GPP,

388   we found that the scenario using the original phenological module presented a larger

389   AET during the period 1979-2000, and the two scenarios simulated AET in the Shrubs

390   dominated region were very close (Fig. 6e-f). The seasonal dynamic patterns of AET in

391   BNS, IBS&TeBS and Shrubs dominated regions are similar. The AET in spring is

392   higher than in summer and autumn when the original phenology module is used. This

393   is because using the original phenology module result in earlier spring phenology. The

394   increase of AET in spring will exacerbates the water stress in summer and autumn

395   through legacy effect, and then reduce AET.
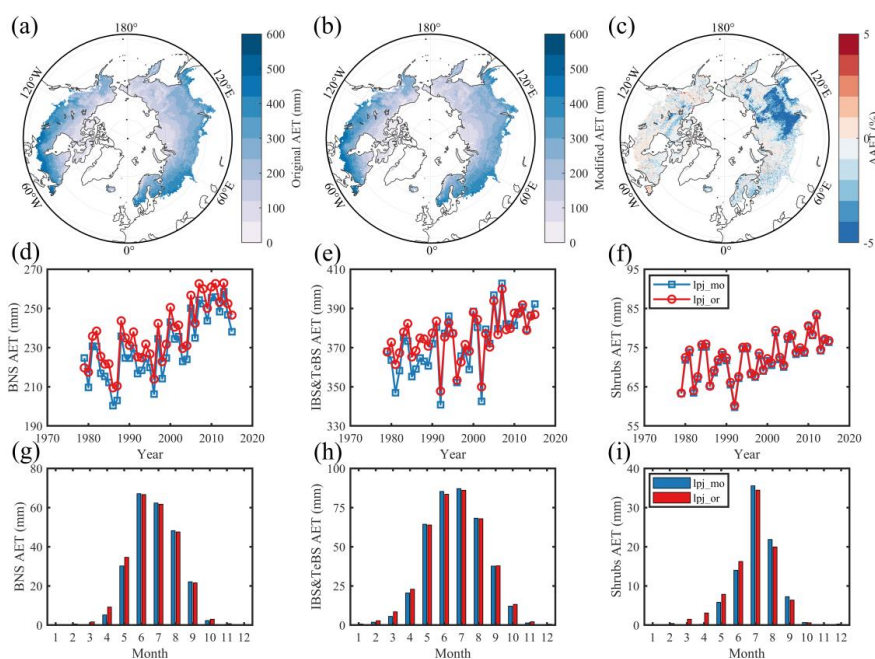
396

397   **Figure 6 Comparison of actual evapotranspiration simulations between scenarios**
398   **which used original phenological module and modified (DROMPHOT and DM)**
399   **phenological module.** (a) Scenario used original phenological module, (b) scenario

400 used modified phenological module, and (c) the difference between the two scenario
401 mentioned above, blue represents a larger simulation value for the LPJ-GUESS model
402 using the original phenological module, and red is smaller. (d-f) Annual average AET
403 for BNS, IBS&TeBS and Shrubs PFTs from 1979 to 2015. (g-i) Multi-year mean
404 monthly AET for BNS, IBS&TeBS and Shrubs PFTs from 1979 to 2015.

405 **4. Discussion**

406 **4.1 Remote Sensing Phenology Facilitates Mixed-Pixel Phenology Modeling**

407 Whether through dynamic global vegetation model simulation or satellite remote

408 sensing extraction, a key issue in large-scale vegetation phenology research is the scale

409 transformation of phenology data in mixed pixels. For phenological extraction based

410 on satellite remote sensing, which is a top-down approach, the spring phenology

411 extracted from the mixed pixel (without specific dominant vegetation types) is the

412 information about the dates when the earliest plant leaf-out occurs in the pixel, while

413 the autumn phenology is the last one to senescence (Chen et al., 2018; Reed et al., 1994;

414 White et al., 2009; Fu et al., 2014). In addition, the greenness of understory phenology

415 (low shrub or grass in forest) further complicates the detecting of overstory signal (Ahl

416 et al., 2006; Tremblay and Larocque, 2001). It is challenging to separate remote sensing

417 signals into different components by filtering or decoupling methods. The more feasible

418 method is to detect phenological changes with few mixed species at a small spatial scale

419 and conducting climate-controlled experiments (Wolkovich et al., 2012).

420 DGVM-based phenological simulation is based on a bottom-up method, different

421 from phenological extraction based on remote sensing. Through simulating plant

422 individuals' growth, development and senescence in the gridcell, which represents

423 different signals in the mixed pixels, and finally synthesizes the vegetation signals of

424 the whole gridcell. In this study, based on top-down remote sensing phenology and

425 parameter calibrations for several relatively pure pixels with clear dominance of BNS,

426 IBS&TeBS and Shrubs PFTs, we integrated these newly calibrated phenology module

427 at PFT level into the LPJ-GUESS to reproduce the gridcell-level vegetation phenology

428 for the mixed pixels. The simulation of vegetation phenology for mixed pixels enables

429 the capture of phenological variability arising from dynamic vegetation changes, as

430 opposed to the predefined approach reliant on specific pixel vegetation types, which

431 also partly explains why phenological models based on predefined vegetation types are

432 difficult to generalize spatially. Leveraging the advantages of wide-ranging remote

433 sensing phenological monitoring and stable monitoring frequencies, analyzing the

434 relationship between pixel constituents and vegetation signals, especially in cases

435 where pixel constituents are relatively uniform, can enhance the accuracy of

436 phenological simulation for mixed pixels.

437 **4.2 Influence of phenological shifts on ecosystem structure**

438 Our results showed that LPJ-GUESS model which using original phenological

439 module estimated earlier SOS in BNS, IBS&TeBS and Shrubs dominant regions than

440 that using the modified phenological module (Fig.3). Earlier spring phenology, which

441 is closely related to plant growth and development and has a strong influence on

442 interspecific competition (Roberts et al., 2015; Rollinson and Kaye, 2012), also lead to

443 a larger dominant area (Fig. S3). In high latitude regions, plants gain a competitive

444 niche when spring phenology advances, which is mediated by the early snowmelt

445 synergistic changes of soil temperature and soil water content, and is manifested in a

446   wider window of high resource availability and low competition (Zheng et al., 2022).

447   During this window period, plants can get more light, water and nutrient resources, and

448   then carry out vegetative growth earlier, and finally increase the leaf area in the spring.

449   As the community develops, changes in competitive relations at the species or

450   functional group level in the spring will induce to changes in community composition

451   (Morisette et al., 2009; Forrest et al., 2010). In the context of climate change,

452   differences in the phenological responses of different species may further affect the

453   distribution of species, and the inaccuracy of future phenological dynamic simulations

454   of different vegetation types in DGVMs will introduce great uncertainty to the

455   estimation of future potential natural plant distribution (Dijkstra et al., 2011).

456   **4.3 Further development of phenological models**

457   Although we have substantially improved the LPJ-GUESS' accuracy of simulating

458   vegetation phenology by coupling calibrated spring (DROMPHT) and autumn (DM)

459   phenological algorithms at PFT levels, we still see the discrepancy in the grass

460   dominated regions, which owing to we did not employ the temperature and photoperiod

461   phenological model for grassland phenology simulation, because many studies indicate

462   that grassland phenology is also regulated by precipitation (Fu et al., 2021).

463   Furthermore, the current phenology algorithms only consider the synergistic effects of

464   temperature and photoperiod, but can be further linked to plant growth and physiology

465   (Fu et al., 2020; Zohner et al., 2023). In different regions (under different external

466   conditions), the driving mechanism and effective driving factors of vegetation

467   phenology process can be different. Temperature is an important factor regulating

468   phenology in energy limited regions, while water supply (precipitation, soil moisture

469   etc.) control cannot be ignored in water limited regions (Prevéy et al., 2017; Fu et al.,

470   2022). For further developing phenological module in DGVMs, on the one hand, it is

471   necessary to carry out mechanism research of phenology of different species through

472   controlled experiments, to the end of improving the existing mechanism model. On the

473   other hand, it is necessary to introduce new methods, such as machine learning, for the

474   accurate generalization of some complex key nonlinear processes (Fu et al., 2020; Dai

475   et al., 2023). Through the above two aspects of work, a comprehensive phenological

476   module can be provided for further improving the accuracy of DGVM models in

477   simulating the phenological dynamics of different PFTs in different environments.

478   **5. Conclusion**

479   In this study, we parameterized and constructed spring (DROMPHOT) and autumn

480   (DM) phenology models for BNS, IBS&TeBS and Shrubs PFTs based on the remote

481   sensing-extracted phenology data. These parameterized DROMPHOT and DM

482   algorithms were further coupled into the LPJ-GUESS model, and the results showed

483   that LPJ-GUESS using the modified phenological module substantially improved in

484   accuracy of spring and autumn phenology compared to the original phenological

485   module. Furthermore, we found that differences in phenological estimations can have

486   significant effects on carbon and water cycling processes by influencing plant annual

487   growth dynamics and ecosystem structure functions. For the carbon cycle, the influence

488   of phenological differences on BNS- and Shrubs-dominated regions was greater than

489   that of IBS&TeBS dominated regions, and there were differences in the seasonality of

490 monthly GPP simulations with different PFTs. For the water cycle, in the BNS-

491 dominant region, the earlier spring phenology leads to an increase in spring AET,

492 leading water stress in summer and autumn through legacy effect, and then reducing

493 AET. We highlighted the importance of phenology estimation and its process

494 interactions in DGVMs and propose further developments in vegetation phenology

495 modeling to improve the accuracy of DGVM models in simulating the phenological

496 dynamics and terrestrial carbon and water cycles.

Geoscientific
Model Development
Discussions

Code and data availability

The code version used for this study is stored in a central code repository and will be made accessible upon request. Details of relevant meteorological driving data and measured verification data can be obtained from the data description section in this paper. VPM GPP product can be download from https://data.nal.usda.gov/dataset/global-moderate-resolution-dataset-gross-primary-production-vegetation-2000%E2%80%932016.

Declaration of Competing Interest

The authors declare that there are no known competing financial interests or personal relationships that influenced the work reported in this paper.

Acknowledgments

Author contributions

518   YHF and JT conceived the ideas and designed methodology; JT provided the

519   modelling help for the LPJ-GUESS and participated in result interpretation and writing;

520   SZC modified the LPJ-GUESS model and analyzed the data and YHF led the writing

521   of the manuscript in corporation with SZC and JT; All authors contributed critically to

522   the drafts and gave final approval for publication.

523

524 **Reference**

525 Ahl, D. E., Gower, S. T., Burrows, S. N., Shabanov, N. V., Myneni, R. B., and Knyazikhin, Y.: Monitoring
526 spring canopy phenology of a deciduous broadleaf forest using MODIS, Remote Sensing of Environment,
527 104, 88-95, 2006.

528 Badeck, F. W., Bondeau, A., Böttcher, K., Doktor, D., Lucht, W., Schaber, J., and Sitch, S.: Responses of
529 spring phenology to climate change, New Phytol., 162, 295-309, 2004.

530 Bartholome, E. and Belward, A. S.: GLC2000: a new approach to global land cover mapping from Earth
531 observation data, Int. J. Remote Sens., 26, 1959-1977, 2005.

532 Caffarra, A., Donnelly, A., and Chuine, I.: Modelling the timing of Betula pubescens budburst. II.
533 Integrating complex effects of photoperiod into process-based models, Climate research, 46, 159-170,
534 2011.

535 Cao, S., Li, M., Zhu, Z., Zha, J., Zhao, W., Duanmu, Z., Chen, J., Zheng, Y., and Chen, Y.:
536 Spatiotemporally consistent global dataset of the GIMMS Leaf Area Index (GIMMS LAI4g) from 1982
537 to 2020, Earth System Science Data Discussions, 1-31, 2023.

538 Chen, S., Fu, Y. H., Hao, F., Li, X., Zhou, S., Liu, C., and Tang, J.: Vegetation phenology and its
539 ecohydrological implications from individual to global scales, Geography and Sustainability, 2022a.

540 Chen, S., Fu, Y. H., Geng, X., Hao, Z., Tang, J., Zhang, X., Xu, Z., and Hao, F.: Influences of Shifted
541 Vegetation Phenology on Runoff Across a Hydroclimatic Gradient, Front. Plant Sci., 12, 802664,
542 10.3389/fpls.2021.802664, 2022b.

543 Chen, S., Fu, Y. H., Wu, Z., Hao, F., Hao, Z., Guo, Y., Geng, X., Li, X., Zhang, X., and Tang, J.: Informing
544 the SWAT model with remote sensing detected vegetation phenology for improved modeling of
545 ecohydrological processes, J. Hydrol., 616, 128817, 2023.

546 Chen, X., Wang, D., Chen, J., Wang, C., and Shen, M.: The mixed pixel effect in land surface phenology:
547 A simulation study, Remote Sensing of Environment, 211, 338-344, 2018.

548 Chuine, I.: A unified model for budburst of trees, Journal of theoretical biology, 207, 337-347, 2000.

549 Chuine, I.: Why does phenology drive species distribution?, Philosophical Transactions of the Royal
550 Society B: Biological Sciences, 365, 3149-3160, 2010.

551 Cong, N., Piao, S., Chen, A., Wang, X., Lin, X., Chen, S., Han, S., Zhou, G., and Zhang, X.: Spring
552 vegetation green-up date in China inferred from SPOT NDVI data: A multiple model analysis, Agric. For.
553 Meteorol., 165, 104-113, 10.1016/j.agrformet.2012.06.009, 2012.

554 Dai, W., Jin, H., Zhou, L., Liu, T., Zhang, Y., Zhou, Z., Fu, Y. H., and Jin, G.: Testing machine learning
555 algorithms on a binary classification phenological model, Global Ecology and Biogeography, 32, 178-
556 190, 2023.

557 Delpierre, N., Dufrêne, E., Soudani, K., Ulrich, E., Cecchini, S., Boé, J., and François, C.: Modelling
558 interannual and spatial variability of leaf senescence for three deciduous tree species in France, Agric.
559 For. Meteorol., 149, 938-948, 2009.

560 Deng, F., Chen, J. M., Plummer, S., Chen, M., and Pisek, J.: Algorithm for global leaf area index retrieval

561 using satellite imagery, IEEE Trans. Geosci. Remote Sens., 44, 2219-2229, 2006.

562 Dijkstra, J. A., Westerman, E. L., and Harris, L. G.: The effects of climate change on species composition,

563 succession and phenology: a case study, Global Change Biol., 17, 2360-2369, 2011.

564 Fang, J. and Lechowicz, M. J.: Climatic limits for the present distribution of beech (Fagus L.) species in

565 the world, J. Biogeogr., 33, 1804-1819, 2006.

566 Forrest, J., Inouye, D. W., and Thomson, J. D.: Flowering phenology in subalpine meadows: Does climate

567 variation influence community co-flowering patterns?, Ecology, 91, 431-440, 2010.

568 Fu, Y., Li, X., Zhou, X., Geng, X., Guo, Y., and Zhang, Y.: Progress in plant phenology modeling under

569 global climate change, Science China Earth Sciences, 63, 1237-1247, 2020.

570 Fu, Y. H., Piao, S., Op de Beeck, M., Cong, N., Zhao, H., Zhang, Y., Menzel, A., and Janssens, I. A.:

571 Recent spring phenology shifts in western C entral E urope based on multiscale observations, Global

572 Ecol. Biogeogr., 23, 1255-1263, 2014.

573 Fu, Y. H., Geng, X., Chen, S., Wu, H., Hao, F., Zhang, X., Wu, Z., Zhang, J., Tang, J., and Vitasse, Y.:

574 Global warming is increasing the discrepancy between green (actual) and thermal (potential) seasons of

575 temperate trees, Global Change Biology, 29, 1377-1389, 2023.

576 Fu, Y. H., Li, X., Chen, S., Wu, Z., Su, J., Li, X., Li, S., Zhang, J., Tang, J., and Xiao, J.: Soil moisture

577 regulates warming responses of autumn photosynthetic transition dates in subtropical forests, Global

578 Change Biol., 28, 4935-4946, 2022.

579 Fu, Y. H., Zhou, X., Li, X., Zhang, Y., Geng, X., Hao, F., Zhang, X., Hanninen, H., Guo, Y., and De

580 Boeck, H. J.: Decreasing control of precipitation on grassland spring phenology in temperate China,

581 Global Ecol. Biogeogr., 30, 490-499, 2021.

582 Geng, X., Zhou, X., Yin, G., Hao, F., Zhang, X., Hao, Z., Singh, V. P., and Fu, Y. H.: Extended growing

583 season reduced river runoff in Luanhe River basin, J. Hydrol., 582, 124538, 2020.

584 Hänninen, H.: Modelling bud dormancy release in trees from cool and temperate regions, 1990.

585 Hickler, T., Smith, B., Sykes, M. T., Davis, M. B., Sugita, S., and Walker, K.: Using a generalized

586 vegetation model to simulate vegetation dynamics in northeastern USA, Ecology, 85, 519-530, 2004.

587 Huang, M., Piao, S., Janssens, I. A., Zhu, Z., Wang, T., Wu, D., Ciais, P., Myneni, R. B., Peaucelle, M.,

588 and Peng, S.: Velocity of change in vegetation productivity over northern high latitudes, Nat. Ecol. Evol.,

589 1, 1649-1654, 2017.

590 Jain, A. K. and Yang, X.: Modeling the effects of two different land cover change data sets on the carbon

591 stocks of plants and soils in concert with CO2 and climate change, Global Biogeochem. Cycles, 19, 2005.

592 Kaufmann, R. K., Zhou, L., Knyazikhin, Y., Shabanov, V., Myneni, R. B., and Tucker, C. J.: Effect of

593 orbital drift and sensor changes on the time series of AVHRR vegetation index data, IEEE Trans. Geosci.

594 Remote Sens., 38, 2584-2597, 2000.

595 Keenan, T. F., Gray, J., Friedl, M. A., Toomey, M., Bohrer, G., Hollinger, D. Y., Munger, J. W., O'Keefe,

596 J., Schmid, H. P., SueWing, I., Yang, B., and Richardson, A. D.: Net carbon uptake has increased through

Geoscientific
Model Development
Discussions

EGU
Open Access

597 warming-induced changes in temperate forest phenology, Nat. Clim. Change, 4, 598-604,
598 10.1038/Nclimate2253, 2014.

599 Kim, J. H., Hwang, T., Yang, Y., Schaaf, C. L., Boose, E., and Munger, J. W.: Warming-induced earlier
600 greenup leads to reduced stream discharge in a temperate mixed forest catchment, J. Geophys. Res.:
601 Biogeosci., 123, 1960-1975, 2018.

602 Kramer, K.: Selecting a model to predict the onset of growth of Fagus sylvatica, J. Appl. Ecol., 172-181,
603 1994.

604 Krinner, G., Viovy, N., de Noblet-Ducoudré, N., Ogée, J., Polcher, J., Friedlingstein, P., Ciais, P., Sitch,
605 S., and Prentice, I. C.: A dynamic global vegetation model for studies of the coupled atmosphere-
606 biosphere system, Global Biogeochem. Cycles, 19, 2005.

607 Kucharik, C. J., Barford, C. C., El Maayar, M., Wofsy, S. C., Monson, R. K., and Baldocchi, D. D.: A
608 multiyear evaluation of a Dynamic Global Vegetation Model at three AmeriFlux forest sites: Vegetation
609 structure, phenology, soil temperature, and CO_2 and H_2O vapor exchange, Ecol. Modell., 196, 1-31,
610 2006.

611 Liu, Q., Fu, Y. H., Liu, Y., Janssens, I. A., and Piao, S.: Simulating the onset of spring vegetation growth
612 across the Northern Hemisphere, Global Change Biol., 24, 1342-1356, 2018.

613 Marini, F. and Walczak, B.: Particle swarm optimization (PSO). A tutorial, Chemometrics and Intelligent
614 Laboratory Systems, 149, 153-165, 2015.

615 Medvigy, D., Wofsy, S., Munger, J., Hollinger, D., and Moorcroft, P.: Mechanistic scaling of ecosystem
616 function and dynamics in space and time: Ecosystem Demography model version 2, J. Geophys. Res.:
617 Biogeosci., 114, 2009.

618 Morales, P., Sykes, M. T., Prentice, I. C., Smith, P., Smith, B., Bugmann, H., Zierl, B., Friedlingstein, P.,
619 Viovy, N., and Sabaté, S.: Comparing and evaluating process-based ecosystem model predictions of
620 carbon and water fluxes in major European forest biomes, Global change biology, 11, 2211-2233, 2005.

621 Morisette, J. T., Richardson, A. D., Knapp, A. K., Fisher, J. I., Graham, E. A., Abatzoglou, J., Wilson, B.
622 E., Breshears, D. D., Henebry, G. M., and Hanes, J. M.: Tracking the rhythm of the seasons in the face
623 of global change: phenological research in the 21st century, Front. Ecol. Environ., 7, 253-260, 2009.

624 Piao, S., Fang, J., Zhou, L., Ciais, P., and Zhu, B.: Variations in satellite-derived phenology in China's
625 temperate vegetation, Global Change Biol., 12, 672-685, 2006.

626 Piao, S., Liu, Q., Chen, A., Janssens, I. A., Fu, Y., Dai, J., Liu, L., Lian, X., Shen, M., and Zhu, X.: Plant
627 phenology and global climate change: Current progresses and challenges, Global Change Biol., 25, 1922-
628 1940, 2019.

629 Pinzon, J. E. and Tucker, C. J.: A non-stationary 1981–2012 AVHRR NDVI3g time series, Remote Sens.,
630 6, 6929-6960, 2014.

631 Poli, R., Kennedy, J., and Blackwell, T.: Particle swarm optimization: An overview, Swarm Intell., 1, 33-
632 57, 2007.

633 Prevéy, J., Vellend, M., Rüger, N., Hollister, R. D., Bjorkman, A. D., Myers-Smith, I. H., Elmendorf, S.

634 C., Clark, K., Cooper, E. J., and Elberling, B.: Greater temperature sensitivity of plant phenology at
635 colder sites: implications for convergence across northern latitudes, Global Change Biol., 23, 2660-2671,
636 2017.

637 Reed, B. C., Brown, J. F., VanderZee, D., Loveland, T. R., Merchant, J. W., and Ohlen, D. O.: Measuring
638 phenological variability from satellite imagery, J. Veg. Sci., 5, 703-714, 1994.

639 Richardson, A. D., Anderson, R. S., Arain, M. A., Barr, A. G., Bohrer, G., Chen, G., Chen, J. M., Ciais,
640 P., Davis, K. J., and Desai, A. R.: Terrestrial biosphere models need better representation of vegetation
641 phenology: results from the N orth A merican C arbon P rogram S ite S ynthesis, Global Change Biology,
642 18, 566-584, 2012.

643 Rinnan, R., Iversen, L. L., Tang, J., Vedel-Petersen, I., Schollert, M., and Schurgers, G.: Separating direct
644 and indirect effects of rising temperatures on biogenic volatile emissions in the Arctic, Proceedings of
645 the National Academy of Sciences, 117, 32476-32483, 10.1073/pnas.2008901117, 2020.

646 Roberts, A. M., Tansey, C., Smithers, R. J., and Phillimore, A. B.: Predicting a change in the order of
647 spring phenology in temperate forests, Global Change Biol., 21, 2603-2611, 2015.

648 Rollinson, C. R. and Kaye, M. W.: Experimental warming alters spring phenology of certain plant
649 functional groups in an early successional forest community, Global Change Biol., 18, 1108-1116, 2012.

650 Ryu, S.-R., Chen, J., Noormets, A., Bresee, M. K., and Ollinger, S. V.: Comparisons between PnET-Day
651 and eddy covariance based gross ecosystem production in two Northern Wisconsin forests, Agric. For.
652 Meteorol., 148, 247-256, 2008.

653 Sarvas, R.: Investigations on the annual cycle of development of forest trees. Active period,
654 Investigations on the annual cycle of development of forest trees. Active period., 76, 1972.

655 Savitzky, A. and Golay, M. J.: Smoothing and differentiation of data by simplified least squares
656 procedures, Anal. Chem., 36, 1627-1639, 1964.

657 Schaefer, K., Collatz, G. J., Tans, P., Denning, A. S., Baker, I., Berry, J., Prihodko, L., Suits, N., and
658 Philpott, A.: Combined simple biosphere/Carnegie-Ames-Stanford approach terrestrial carbon cycle
659 model, J. Geophys. Res.: Biogeosci., 113, 2008.

660 Sellers, P., Mintz, Y., Sud, Y. e. a., and Dalcher, A.: A simple biosphere model (SiB) for use within general
661 circulation models, J. Atmos. Sci., 43, 505-531, 1986.

662 Sellers, P., Randall, D., Collatz, G., Berry, J., Field, C., Dazlich, D., Zhang, C., Collelo, G., and Bounoua,
663 L.: A revised land surface parameterization (SiB2) for atmospheric GCMs. Part I: Model formulation, J.
664 Clim., 9, 676-705, 1996.

665 Sitch, S., Smith, B., Prentice, I. C., Arneth, A., Bondeau, A., Cramer, W., Kaplan, J. O., Levis, S., Lucht,
666 W., and Sykes, M. T.: Evaluation of ecosystem dynamics, plant geography and terrestrial carbon cycling
667 in the LPJ dynamic global vegetation model, Global Change Biol., 9, 161-185, 2003.

668 Sykes, M. T., Prentice, I. C., and Cramer, W.: A bioclimatic model for the potential distributions of north
669 European tree species under present and future climates, Journal of Biogeography, 203-233, 1996.

670 Tang, J., Zhou, P., Miller, P. A., Schurgers, G., Gustafson, A., Makkonen, R., Fu, Y. H., and Rinnan, R.:

671 High-latitude vegetation changes will determine future plant volatile impacts on atmospheric organic
672 aerosols, npj Climate and Atmospheric Science, 6, 147, 2023.

673 Thornton, P. E., Law, B. E., Gholz, H. L., Clark, K. L., Falge, E., Ellsworth, D. S., Goldstein, A. H.,
674 Monson, R. K., Hollinger, D., and Falk, M.: Modeling and measuring the effects of disturbance history
675 and climate on carbon and water budgets in evergreen needleleaf forests, Agric. For. Meteorol., 113, 185-
676 222, 2002.

677 Tremblay, N. O. and Larocque, G. R.: Seasonal dynamics of understory vegetation in four eastern
678 Canadian forest types, International Journal of Plant Sciences, 162, 271-286, 2001.

679 Tucker, C. J., Pinzon, J. E., Brown, M. E., Slayback, D. A., Pak, E. W., Mahoney, R., Vermote, E. F., and
680 El Saleous, N.: An extended AVHRR 8-km NDVI dataset compatible with MODIS and SPOT vegetation
681 NDVI data, Int. J. Remote Sens., 26, 4485-4498, 2005.

682 Viovy, N.: CRUNCEP version 7-atmospheric forcing data for the community land model, 2018.

683 White, M. A., Thornton, P. E., and Running, S. W.: A continental phenology model for monitoring
684 vegetation responses to interannual climatic variability, Global Biogeochem. Cycles, 11, 217-234, 1997.

685 White, M. A., de Beurs, K. M., Didan, K., Inouye, D. W., Richardson, A. D., Jensen, O. P., O'keefe, J.,
686 Zhang, G., Nemani, R. R., and van Leeuwen, W. J.: Intercomparison, interpretation, and assessment of
687 spring phenology in North America estimated from remote sensing for 1982–2006, Global Change
688 Biology, 15, 2335-2359, 2009.

689 Wolkovich, E. M., Cook, B. I., Allen, J. M., Crimmins, T., Betancourt, J. L., Travers, S. E., Pau, S.,
690 Regetz, J., Davies, T. J., and Kraft, N. J.: Warming experiments underpredict plant phenological
691 responses to climate change, Nature, 485, 494-497, 2012.

692 Zani, D., Crowther, T. W., Mo, L., Renner, S. S., and Zohner, C. M.: Increased growing-season
693 productivity drives earlier autumn leaf senescence in temperate trees, Science, 370, 1066-1071, 2020.

694 Zhang, Y., Commane, R., Zhou, S., Williams, A. P., and Gentine, P.: Light limitation regulates the
695 response of autumn terrestrial carbon uptake to warming, Nat. Clim. Change, 10, 739-743, 2020.

696 Zheng, J., Jia, G., and Xu, X.: Earlier snowmelt predominates advanced spring vegetation greenup in
697 Alaska, Agric. For. Meteorol., 315, 108828, 2022.

698 Zhou, X., Geng, X., Yin, G., Hänninen, H., Hao, F., Zhang, X., and Fu, Y. H.: Legacy effect of spring
699 phenology on vegetation growth in temperate China, Agric. For. Meteorol., 281, 107845, 2020.

700 Zhu, Z., Piao, S., Myneni, R. B., Huang, M., Zeng, Z., Canadell, J. G., Ciais, P., Sitch, S., Friedlingstein,
701 P., and Arneth, A.: Greening of the Earth and its drivers, Nat. Clim. Change, 6, 791-795, 2016.

702 Zohner, C. M., Mirzagholi, L., Renner, S. S., Mo, L., Rebindaine, D., Bucher, R., Palouš, D., Vitasse, Y.,
703 Fu, Y. H., and Stocker, B. D.: Effect of climate warming on the timing of autumn leaf senescence reverses
704 after the summer solstice, Science, 381, eadf5098, 2023.

705